

Distribution Agreement:

In presenting this thesis as a partial fulfillment of the requirements for a degree from Emory University, I hereby grant to Emory University and its agents the non-exclusive license to archive, make accessible, and display my thesis in whole or in part in all forms of media, now or hereafter now, including display on the World Wide Web. I understand that I may select some access restrictions as part of the online submission of this thesis. I retain all ownership rights to the copyright of the thesis. I also retain the right to use in future works (such as articles or books) all or part of this thesis.

Suyeon Kim

March 28, 2021

The Effects of Amino Acid Substitutions on MCL-1 Protein Structure and Function

By

Suyeon Kim

Lawrence H. Boise

Advisor

Department of Biology

Lawrence H. Boise

Advisor

Anita Corbett

Committee Member

LaTonia Taliaferro-Smith

Committee Member

2021

The Effects of Amino Acid Substitutions on MCL-1 Protein Structure and Function

By

Suyeon Kim

Lawrence Boise

Advisor

An abstract of
a thesis submitted to the Faculty of Emory College of Arts and Sciences
of Emory University in partial fulfillment
of the requirements of the degree of
Bachelor of Science with Honors

Department of Biology

2021

ABSTRACT

The Effects of Amino Acid Substitutions on MCL-1 Protein Structure and Function By Suyeon Kim

Multiple myeloma (MM) is a B-cell malignancy that makes up 1% of all diagnosed cancers. Recent studies have outlined MM molecular mechanisms, such as the intrinsic apoptotic pathway regulated by the BCL-2 family of proteins. In the pathway, MCL-1 is an essential anti-apoptotic protein vital for cell maintenance, survival, and regulated cell death. Further, the BH regions of the MCL-1 protein form a binding pocket in which BH3 sensitizers and targeted therapy drugs can bind to induce apoptosis. Specifically, BH3-mimetics are small, lipophilic molecules that induce apoptosis in cancer cells. BIM is a pro-apoptotic BH3-only activator protein that is sequestered by MCL-1 to inhibit the activation of pro-apoptotic proteins BAK & BAX, ultimately inhibiting MOMP and apoptosis. In this study, three BIM bound MCL-1 complexes (2PQK, 6QFI, & 2KBW) & four drug inhibitor bound MCL-1 complexes (Servier S63845 (5LOF), Servier 2019 (6QYP), preliminary AMG-176 compounds (6OQC & 6OQB), and AstraZeneca (6FS0)) were investigated. The purpose of this investigation is to analyze the effects of MCL-1 amino acid substitutions found in newly diagnosed MM patients (V249L, L267V, N223S, and R214Q) and various other malignancies (V216I, V216L, V258L, and L267F) on the protein's structure and function.

The alignment feature on PyMOL was utilized to display changes in the amino acid side chains between the WT and mutant variants. In particular, the MCL-1^{L267V} amino acid substitution displayed changes in the side chain that may have implications for the binding of drug inhibitors and BIM. Distance measurements revealed that Val267 associated with MCL-1^{L267V} was found to be closer in proximity to all drug inhibitors (6OQC, 6OQB, 6FS0, 5LOF, and 6QYP); however, the Val267 side chain was also found to be further in distance to all the BIM molecules (2PQK, 6QFI, and 2KBW). These results may indicate that the MCL-1^{L267V} mutation prevents the binding of drug inhibitors to MCL-1 & BIM displacement from MCL-1. Although the side chain substitutions are conserved in size and property, the L267V mutation is not exempt from phenotypic implications as these mutations alter the space available between the binding pocket and drug inhibitors & BIM molecules.

Taken together, the data suggests that MCL-1 mutations may affect the protein's interaction with drug inhibitors and alter the downstream intrinsic apoptotic pathway. As a protein that interacts directly with BH3 sensitizer drugs and is important for cell survival, it is imperative that MCL-1 protein targeting therapy and the molecular mechanism of MM is further investigated.

The Effects of Amino Acid Substitutions on MCL-1 Protein Structure and Function

By

Suyeon Kim

Lawrence Boise

Advisor

A thesis submitted to the Faculty of Emory College of Arts and Sciences
of Emory University in partial fulfillment
of the requirements of the degree of
Bachelor of Science with Honors

Department of Biology

2021

Acknowledgements:

I would like to express my gratitude towards my mentor & advisor, Dr. Lawrence Boise, for his patient advice and guidance throughout this research process.

I would also like to acknowledge the members of the Boise Lab (Shannon Matulis, Vikas Gupta, Benjamin Barwick, David Weir, Tyler Moser-Katz, James Ackley, and Becca Owens) for their constant support and encouragement throughout my time in the lab.

Finally, I would like to thank my committee members, Dr. LaTonia Taliaferro-Smith & Dr. Anita Corbett, for serving on my thesis committee.

Table of Contents:

Introduction	1
Figure 1.....	7
Figure 2.....	8
Figure 3.....	9
Figure 4.....	10
Figure 5.....	11
Figure 6.....	12
Figure 7.....	13
Methods & Materials	14
Results	17
Figure 8.....	24
Figure 9.....	25
Figure 10.....	26
Table 1.....	27
Table 2.....	28
Figure 11.....	29
Figure 12.....	30
Figure 13.....	31
Figure 14.....	32
Figure 15.....	33
Figure 16.....	34

Discussion	35
Conclusion	38
Supplementary Information	39
References	41

INTRODUCTION:

Multiple myeloma (MM) is a B-cell malignancy that makes up 1% of all diagnosed cancers¹ and is the second most common of all hematological malignancies². While accounting for 15% of all lymphohematopoietic cancers, MM disproportionately affects African American men³. Findings on the etiology and environmental risk factors of this plasma cell neoplasm are inconsistent and largely unknown. However, recent studies have outlined the molecular mechanisms that account for MM tumor cell growth, migration, and survival in the bone marrow⁴. These studies have provided a framework for novel targeted therapies and mechanisms that inhibit MM cell growth⁵.

The intrinsic, mitochondrial, apoptotic pathway in MM is regulated by the interaction of BCL-2 family proteins at the mitochondrial outer membrane⁶. The BCL-2 family of proteins includes anti-apoptotic proteins (BCL-X_L & MCL-1), pro-apoptotic effector proteins (BAK & BAX), pro-apoptotic BH3-only activator proteins (BIM & BID & PUMA), and BH3 sensitizer proteins (NOXA)⁷. Apoptosis in particular is mediated through BCL-2 proteins' regulation of mitochondrial outer membrane permeabilization (MOMP)⁸. The BCL-2 homology domain 3 (BH3) region is part of an essential interaction region between the BH3-only proteins and relatives of the BCL-2 family that regulate MOMP⁹. Specifically, BH3 sensitizer proteins prime the cell for apoptosis by releasing BH3-only activator proteins from anti-apoptotic proteins such as MCL-1¹⁰. The pro-apoptotic effector proteins BAX & BAK are activated by the BH3-only activators (BIM & BID), which oligomerize and results in MOMP¹¹. In summary, apoptosis requires the availability of both

anti-apoptotic (MCL-1, BCL-2, BCL-XL) and pro-apoptotic proteins (BAK, BAX, BIM, & BID)¹² (Figure 1). Consequently, cytochrome c is released from the mitochondria into the cytosol, initiating apoptosome formation, caspase activation, and intrinsic apoptosis¹³. However, apoptosis is deregulated in cancerous cells, and anti-apoptotic protein expression levels are high. Apoptotic activity of BAK & BAX is inhibited through direct binding of pro-apoptotic proteins or BH3-only activators to anti-apoptotic proteins such as MCL-1¹⁴. In sum, apoptotic inhibitors that balance and regulate the activity of pro-apoptotic proteins can also contribute to the resistance to cell death observed in cancer cells.

Of the anti-apoptotic proteins, the 3D structure of MCL-1's is notable. Like all BCL-2 family proteins, MCL-1 contains BH regions BH4, BH3, BH1, and BH2 respectively from the N to C terminus¹⁵ (Figure 2). The protein is comprised of nine alpha helices in which $\alpha 1$ is associated with the BH4 domain, $\alpha 2$ is associated with the BH3 domain, $\alpha 4$ & $\alpha 5$ are associated with the BH1 domain, $\alpha 7$ & $\alpha 8$ are associated with the BH2 domain, and $\alpha 9$ is associated with the transmembrane domain that holds MCL-1 to the mitochondrial membrane¹⁶⁻¹⁸. Additionally, there are four binding pockets (P1-P4) that make up the hydrophobic groove^{19,20}. The Arg263 residue found in P2 is a hotspot that forms protein-protein interactions with binding ligands – specifically forming salt bridges with corresponding Asp residues on BH3-only proteins¹⁷. These specific MCL-1 regions affect ligand binding and are conserved across all anti-apoptotic proteins. For MCL-1 in particular, P2 & P3 have the most interactions with binding ligands²¹. Moreover, P2 in MCL-1 is flexible and adaptable – expanding to form a hydrophobic cavity in the presence of a

ligand. MCL-1 is also unique in that the hydrophobic groove is lined with Lys and His, making the pocket slightly electropositive²².

The role of MCL-1 protein is also notable within the BCL-2 family. The *MCL-1* locus is located on the 1q21 arm and the encoded protein includes a proline (P), glutamate (E), serine (S), and threonine (T) rich region (PEST) near the N-terminus²³. The PEST domain regulates MCL-1 protein degradation and accounts for the high turnover rate of MCL-1^{23,24}. Beyond the PEST domain on the MCL-1 protein are the four BCL-2 homology (BH1-BH4) domains²⁵. This BH domain is made up of amphipathic alpha helices that are in close proximity to each other, forming a pocket for the binding of proapoptotic activator proteins and drug inhibitors²⁶. In addition to its distinct structure, MCL-1 is indispensable to the survival of lymphocytic cell lines²⁷. Furthermore, MCL-1 levels are overexpressed, associated with relapse & shorter survival for MM patients, and linked with increased levels of drug resistance and cell survival²⁸. Specifically in MM, 40% of newly diagnosed patients display a copy gain of the 1q21 chromosome²⁹. This 1q21 amplification is not only associated with poor survival but is also correlated with increased MCL-1 mRNA expression levels (Figure 3). MCL-1 is an essential anti-apoptotic protein for MM cell maintenance, survival, and regulated cell death.

BIM is a pro-apoptotic BH3-only activator protein that is sequestered by MCL-1 to inhibit the activation of pro-apoptotic proteins BAK & BAX, ultimately inhibiting MOMP and apoptosis. As the name suggests, BH3 is the only one of the four BH domains present in BH3-only activator proteins like BIM. The BH3 domain present in BIM is an amphipathic

alpha helix that interacts with the hydrophobic groove in anti-apoptotic proteins such as MCL-1³⁰. Additionally, four hydrophobic residues (h1: I90, h2: L94, h3: I97, and h4: F101) and residue site Asp99 are conserved on the BH3 domain of BIM³¹. The h1-h4 residues lie on the same face of the BH3 domain on BIM's alpha helix, allowing the structure to engage with the four corresponding binding pockets (P1-P4) on MCL1. Furthermore, the Asp99 residue on BIM forms a salt bridge with Arg263 on MCL-1¹⁷. In the intrinsic apoptotic pathway, BH3 sensitizers and drug inhibitors displace pro-apoptotic activators (BIM & BID) from the MCL-1 protein to activate apoptosis¹². In particular, the binding of BIM has been associated with MCL-1 protein stabilization³². In this study, three BIM bound MCL-1 complexes were investigated: 2PQK, 6QFI, & 2KBW (Figure 4).

BH3-mimetics are lipophilic, small molecules that mimic the activity of Noxa and other BH3 sensitizer proteins and induce apoptosis in cancer cells³³. These drug inhibitors overcome apoptosis resistance by displacing the pro-apoptotic BH3-only activator proteins (BIM, BID, & PUMA) on the BH3 anti-apoptotic proteins (MCL-1 & BCL-XL). More specifically, BH3 mimetic drugs compete for the pro-survival protein's hydrophobic groove to antagonize the protein's anti-apoptotic function³⁴. The large, hydrophobic binding pocket has been an obstacle in the development of BH3 mimetics and their inhibition of anti-apoptotic proteins⁶. Despite the initial reservations, several BH3 mimetic drugs, most notably Venetoclax, have been designed³⁵. There are several BH3 mimetics under examination for use in various malignancies that selectively target MCL-1³⁶. Currently, there are four MCL-1 targeting compounds that have shown preclinical efficacy: VU551013 from Vanderbilt University for Acute Myeloid Leukemia (AML), S64315 from Servier &

Novartis for AML & myelodysplastic syndrome, AMG-176 from Amgen for AML and MM, and AZD5991 from AstraZeneca for chronic lymphocytic leukemia and MM¹⁷. In this study, the Servier S63845 (5LOF), Servier 2019 (6QYP), preliminary AMG-176 compounds (6OQC & 6OQB), and AstraZeneca (6FS0) MCL-1 drug inhibitors were studied (Figure 4).

The Multiple Myeloma Research Foundation's CoMMpass database records genetic sequencing data from over 1000 MM patients worldwide. The Interim Analysis 13 MMRF CoMMpass study was previously used to determine the frequency of nonsynonymous coding mutations in the BCL-2 gene family. The analysis from a baseline sample of 982 patients revealed that there were no detected mutations in the pro-apoptotic effector genes (BAK & BAX) and BH3-only genes (BIM & BID). However, *MCL-1* was mutated in 10 baseline samples (1.02%) and was often clonal (variant allele frequency: median 0.391 & range 0.066 – 0.531) (Figure 5). Of the five myeloma missense mutations in proximity to the functional BH1/BH3 binding pocket domain (L186F, R214Q, N223S, V249L, and L267V), the *MCL-1*^{L267V} mutation resulted in decreased sensitivity to cell death when exposed to MCL-1 drug inhibitor S64315 in the murine B-ALL cell line (Figure 6A). Furthermore, all five myeloma mutations resulted in resistance to cell death when exposed to drug inhibitor AZD5991 with *MCL-1*^{L267V} resulting in the greatest resistance to cell death (Figure 6B). Upon closer inspection, the L267V mutation prevented the binding of drug inhibitors to the MCL-1 protein and/or blocked the ability of drug to displace pro-apoptotic proteins required to induce cell death (Figure 7).

In order to study these missense mutations, the wildtype and mutant MCL-1 proteins in complex with drug inhibitors and BIM were modeled using PyMOL. The five myeloma missense mutations in proximity to the functional BH1/BH3 binding pocket domain (L186F, R214Q, N223S, V249L, and L267V) were investigated alongside five non-myeloma mutation sites on *MCL-1* (V216I, V216L, V257I, V258L, and L267V). The purpose of this experiment was to predict the effects of myeloma specific *MCL-1* mutations on protein function and drug binding. The hypothesis is that amino acid substitutions in the MCL-1 protein will decrease MCL-1 protein stability. It is predicted that by comparing the WT MCL-1 protein structure to the mutated structures, MCL-1's interactions with BH3 mimetic drugs, BCL-2 family relative proteins, and even cell survival will be affected. As a protein that interacts directly with BH3 sensitizer drugs and cell survival, it is imperative that MCL-1 molecular mechanisms and targeted therapies are further investigated.

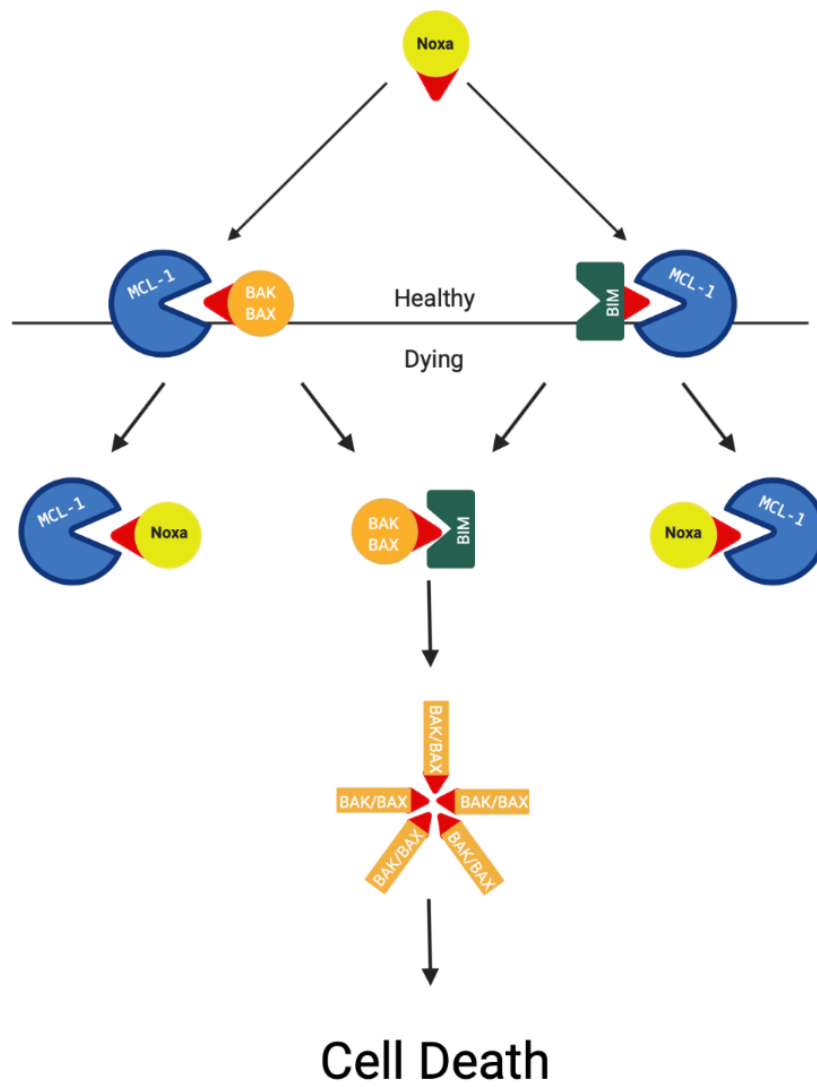


Figure 1. Simplified Intrinsic Apoptotic Pathway Schematic.

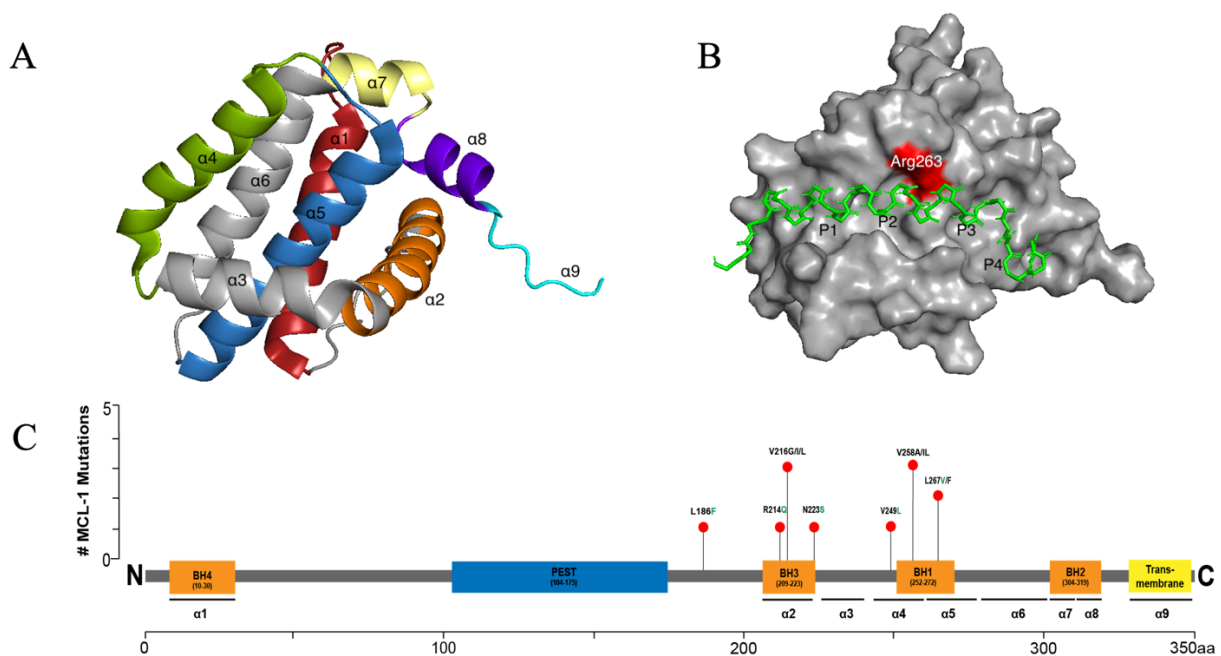


Figure 2. The 3D structure of MCL-1 protein is comprised of **(A)** nine alpha helices and **(B)** four binding pockets (P1-P4) that make up the hydrophobic groove. Arg263 is hotspot for protein-protein interactions between MCL-1 and binding ligands. **(C)** Five MCL-1 myeloma missense mutations (L186F, R214Q, N223S, V249L, & L267V) together with missense mutations from various malignancies (V216G/I/L, V258A/I/L, & L267F) were investigated for a total of twelve missense mutations along the BH3 & BH1 domain representing the MCL-1 binding pocket groove.

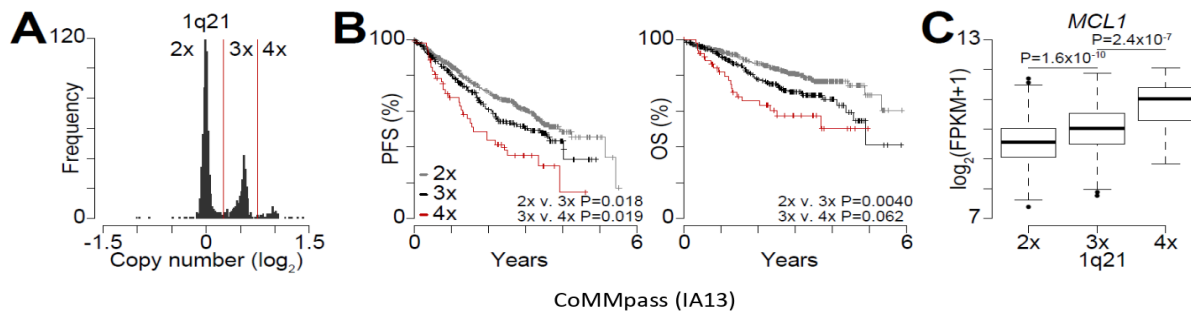


Figure 3. MMRF CoMMpass study (Interim Analysis 13) on MCL-1 copy number variations. MCL-1 is located on the 1q21 region. 1q21 arm copy number frequencies (**A**) and their effects on the overall and progression free survival (**B**) of multiple myeloma patients display a decrease in survival. (**C**) MCL-1 mRNA levels were also affected by MCL-1 copy numbers in myeloma patients, displaying dose dependence. Figures A & B derived from Schmidt et al. (2019): <https://www.nature.com/articles/s41408-019-0254-0>

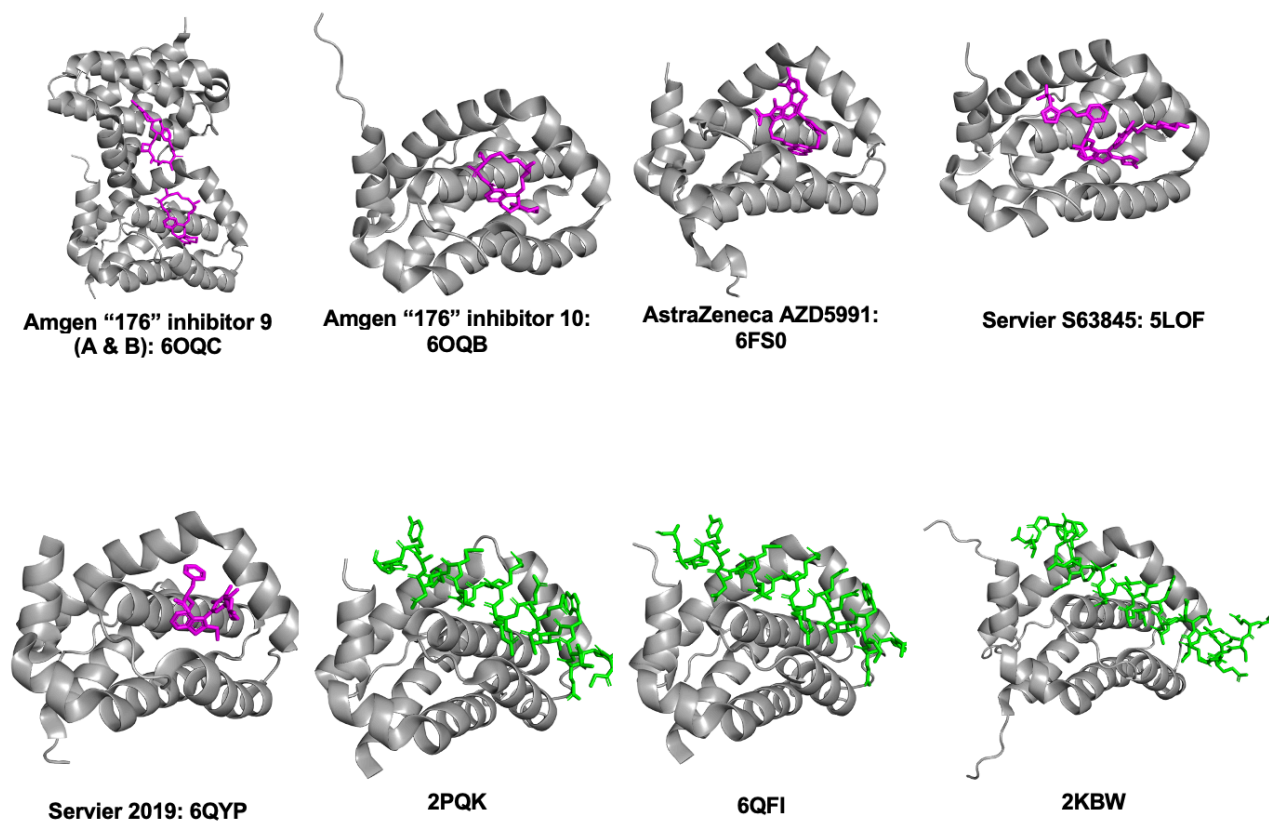


Figure 4. Drug inhibitors (pink) & BIM activators (green) in complex with MCL-1 protein.

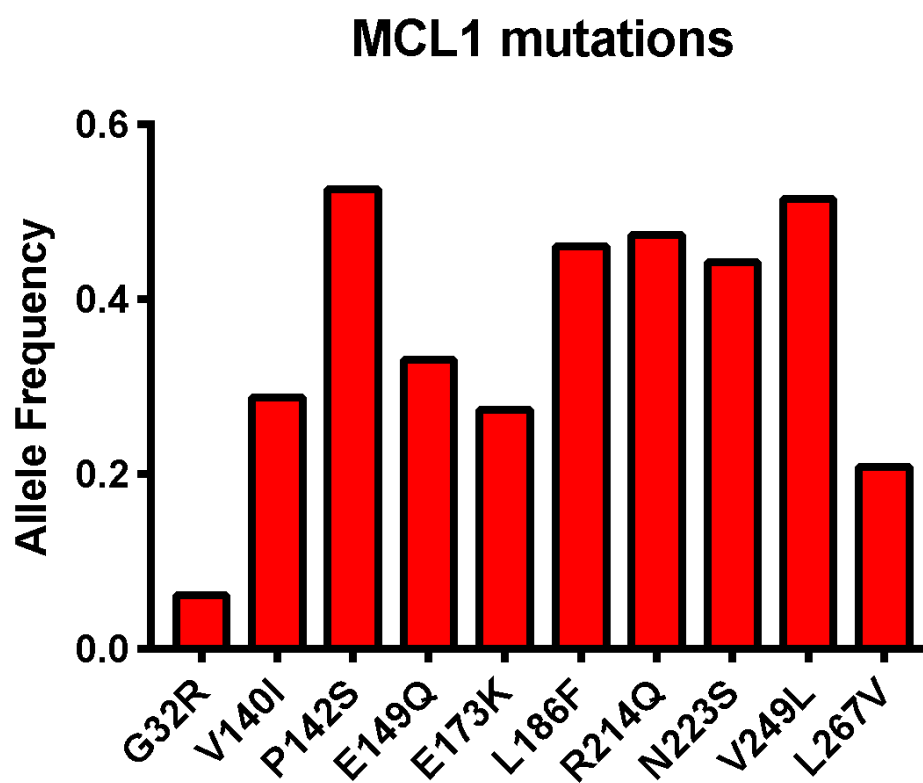


Figure 5. CoMMpass Interin Analysis 13 conducted by Lawrence Boise, PhD & Brandon Chen, B.S.

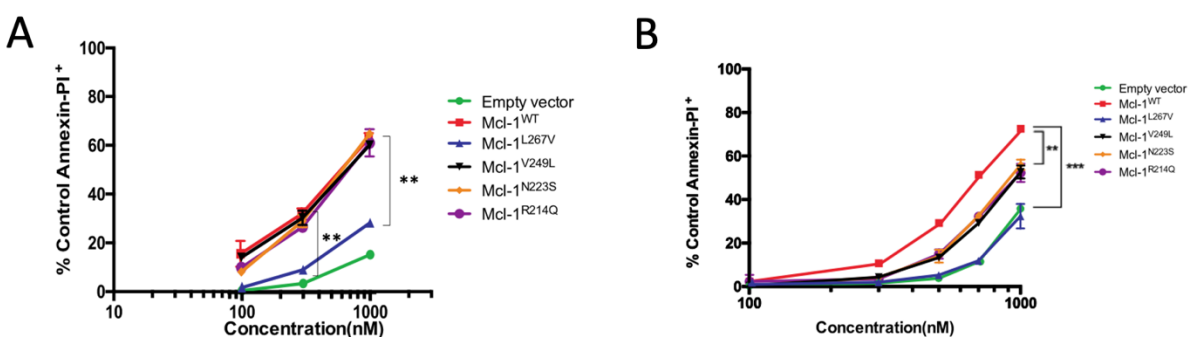


Figure 6. S63845-induced cell death is attenuated in cell expression MCL1^{L267V} & AZD5991 activity is impacted by additional MCL-1 mutations. (A) B-All cells with empty vector and different MCL1 constructs got subject to 100, 300, and 1000 nM of S63856. Cell viability was measured through Annexin-V/PI staining 24 hours post treatment. *** indicates P value <0.001. **** indicates P value <0.001. Data shown are a mean of 3 independent experiments. Statistical significance was assessed using two-tailed t-test using GraphPad. **(B)** WT cells were highly sensitive to MCL1 inhibition and L267V mutation was completely resistant to AZD5991-induced apoptosis. The remaining 3 mutations also resulted in diminished killing activity when compared to cells expressing the WT MCL1. Data shown are a mean of 3 independent experiments. Statistical significance was assessed using two-tailed t-test using GraphPad. ** indicates P value < 0.01. *** indicates P value < 0.001. Studies conducted by Brandon Chen, B.S.

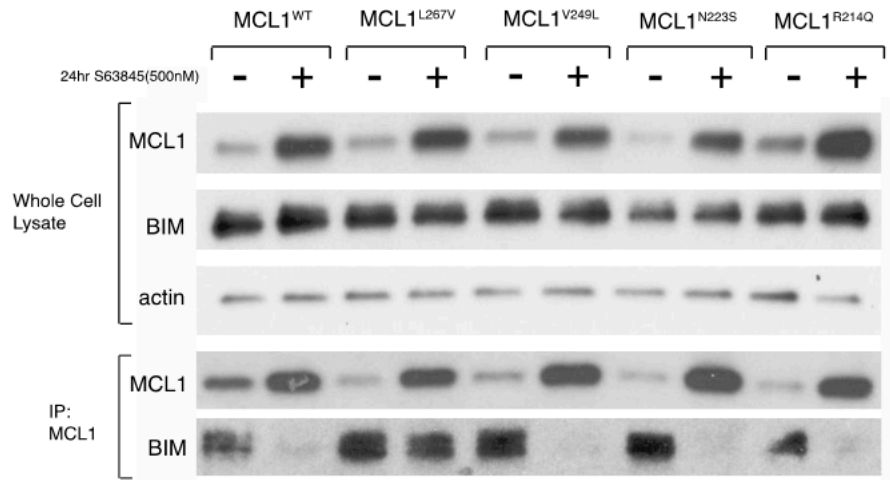


Figure 7. MCL-1^{L267V} is stabilized by S63845 similar to MCL-1^{WT} but does not induce the release of BIM bound to the mutant. We collected protein lysate from B-ALL cells expressing different MCL-1 constructs after 24 hours of S63845 treatment. We subjected the protein lysate to co-immunoprecipitation of MCL-1 and kept the whole cell lysate as a control. MCL-1, BIM, and actin protein expression levels were probed with respective antibodies. The IP results indicated the L267V mutation disabled MCL-1 to release BIM when treated with S63845 unlike wild-type and other mutants. Study conducted by Brandon Chen, B.S.

METHODS & MATERIALS:

Cell Culture

The OCI-MY5-Cas 9, KMS18-Cas 9, and KMS PE 12 – Cas9 cell lines were regularly maintained in Dulbecco's Modification of Eagle's Medium supplemented with 10% Fetal Bovine Serum, 100 unit/mL penicillin/streptomycin, 2 mM L-glutamate, and 1% HEPES buffer. Cells were cultured in humidified incubators at 37°C with 5% carbon dioxide.

Designing sgRNA Guides

Guide RNA sites were designed using CRISPOR (<http://crispor.tefor.net>). Areas spanning the exon-intron regions and the promoter were identified, and sgRNA sites with a specificity score of at least 50 were selected for further investigation. Three guides were selected to improve chances of having a functional sgRNA. Guide RNA site designs were conducted by Ben Barwick, PhD.

PCR Overlap Extension Cloning

MCL-1 sgRNA – specific forward and reverse primers were designed and used in overlap extension PCR to clone the sgRNA into the target vector. A double digestion of pLX_sgRNA plasmid was performed with restriction enzymes XhoI and NheI. Then the PCR overlap extension product was ligated into the cut sites. Competent JM109 cells were then transformed with ligated plasmid on ampicillin agar plates. Purified plasmid DNA from the transformed JM109 cells were sequenced to confirm sgRNA presence.

MM Cell Line Lenti-Viral Infection

HEK293T cells were transfected to produce viral sgRNA plasmid supernatant. The lentiviral supernatant was harvested and used to infect dox-inducible Cas9 expressing myeloma cells. More specifically, OCI-My5-Cas9, KMS18-Cas9, and KMS PE 12-Cas9 cell lines were transfected. Blasticidin selection was used to isolate transduced cell.

Generation of pBABE-MCL-1 Constructs

MCL-1 coding region sequence was cloned into pBABE-puro using the recognition sites of BamHI and EcoRI. pBABE-puro was a gift from Hartmut Land & Jay Morgenstern & Bob Weinberg (Addgene plasmid # 1764). The missense mutations L267V, V249L, N223S, R214Q in *MCL-1* were generated by site-directed mutagenesis using QuikChange II XL Site-Directed Mutagenesis Kit from Agilent, following the manufacturer's protocol. Mutagenesis primers were designed using the QuikChange® Primer Design Program. The mutagenesis primers' sequences are as follows:

L267V – 5' ACT GGG GCA GGA TTG TGA CTG TCA TTT CTT TTG G 3' AND 5' CCA AAA GAA ATG ACA GTC ACA ATC CTG CCC CAG T 3' ; V249L – 5' CTG AAA ACA TGG ATC ATC AAT CGA GAC AAC GAT TTC ACA TCG 3' AND 5' CGA TGT GAA ATC GTT CTC TCG ATT GTA GAT CCA TGT TTT CAG 3' ; N223S – 5; CCG TCT CGT GGC TGC GCT GCA CGC C 3' AND 5' GGC GTG CAG CGC AGC CAC GAG ACG G 3' ; R214Q – 5' GCG CTG GAG ACC TTA CAA CGG CTT GGG G 3'.

Site-directed mutagenesis products were sent for sequencing to confirm the incorporation of the intended mutations. Generation of mutant *MCL-1* was conducted by Pamela Wong, BS.

CbioPortal

CbioPortal was used to identify additional missense mutations in the *MCL-1* gene for further investigation with the five MM MCL-1 missense mutation (L186F, R214Q, N223S, V249L, and L267V). The mutation sites identified on CBioPortal to study along with the five MM mutation sites are: V216I, V216L, V258I, V258L, and L267F.

Python Script & PyMOL

Protein modeling program PyMOL was utilized to create 3D structures of the MCL-1 proteins and their mutations. PyMOL's alignment feature was utilized to highlight the changes between the WT and mutant MCL-1 protein structures and visualize the protein's change in structure in the presence of MCL-1 inhibitor drugs & BIM. Additionally, the PyMOL models of MCL-1 mutations, inhibitor drugs, and BIM were analyzed for the proximity of MCL-1 mutations to the drug inhibitors & BIM. A Python script (Supplementary Information) utilizing the pairwise distance analysis was coded to determine the closest distance from a mutation site to the drug inhibitors and BIM.

RESULTS:

PCR Overlap Extension

To study the functional effects of the myeloma missense mutations in human cell lines and effort was made to insert mutant MCL-1 constructs then knock out endogenous MCL-1 protein in KMS12PE CAS9, OCIMY5 CAS9, and KMS18 CAS9 cell lines. In order to knock out endogenous MCL-1 protein, sgRNA guides were designed and molecularly cloned. PCR overlap extension was performed to clone the designed guide RNA (Figure 8) into the pLX_sgRNA plasmid at XhoI and NheI digestion enzyme cut sites. An ethidium bromide gel was run with digested pLX_sgRNA to visualize the results of the PCR overlap extension and restriction enzyme digest (Figure 9). The pLX_sgRNA resulted in two bands – one between 400 base pairs and 500 base pairs and the second over 2000 base pairs in size. PCR overlap extension products of guide RNA sites MCL1.tss1, MCL1.i2e2, and MCL1.e3i2 all resulted in a single band between 400 and 500 base pairs (Figure 9). The pLX_sgRNA plasmid (7477 bp) contains restriction enzyme sites XhoI (located at 2848 bp within the plasmid) and NheI (located at 3309 bp within the plasmid). The XhoI and NheI region was excised from the pLX_sgRNA plasmid through restriction enzyme digestion. Figure 9 displays the verification of proper digestion with ethidium bromide gels, in which the pLX_sgRNA column displays two bands with approximately 450bp and greater than 2000 bp molecular length. The XhoI and NheI region is 461 bp and the remaining plasmid is 7016 bp in length, confirming that there was a proper digestion at the XhoI and NheI cut sites.

In addition, the MCL1.tss1, MCL1.i2e2, and MCL1.e3i2 columns display the overlap extension PCR products (Figure 9). Each column contains a single band, which are all approximately 450 bp in length. The single band shows that the PCR products were pure and that the products are approximately the same size as the XhoI and NheI region. This is significant as the PCR product sgRNA can replace the XhoI and NheI region in the pLX_sgRNA plasmid as they are approximately the same length.

JM109 Competent Cell Transformation

Competent JM109 cells were transformed and grown out on ampicillin agar plates. The plasmids were isolated from the bacteria using miniprep (Sigma-Aldrich). Purified plasmid DNA from the transformed cells were sequenced from Psomagen Inc. to confirm the presence of the sgRNA. Sequencing results from Psomagen Inc. confirmed that MCL1.tss1, MCL1.i2e2, and MCL1.e3i2 plasmid DNA samples all contained sgRNA sites.

Drug inhibitors & BIM change MCL-1 structure

Published structures of drug inhibitor bound MCL-1 (6OQC, 6OQB, 6FS0, 5LOF, and 6QYP) were overlaid over published structures of BIM bound MCL-1 on PyMOL using the alignment feature. The alignment displayed a change in MCL-1 structure when BIM is bound to the protein. More specifically, $\alpha 2$ shifted upward in the direction of the Arg263 residue or shifted upward and to the right towards the BIM molecule (Figure 10A). $\alpha 3$ shifted in a clockwise rotation with a constant center at the helix's median (Figure 10B).

The distances at “segment 1” (Ala227 to Val253), “segment 2” (Met231 to Val249), and “segment 3” (Lys234 to Leu246) between $\alpha 3$ and $\alpha 4$ were measured for the empty MCL-1 model (2MHS), MCL-1 models with drug inhibitors (6FS0, 5LOF, 6QYP, & 6OQC), and MCL-1 models bound to BIM (2PQK, 6QFI, & 2KBW) (Figure 10C-10J). When compared to the empty MCL-1 structure, the binding of drug inhibitors to MCL-1 widened the binding pocket at segments 1 & 2 (average increase of 0.90 & 4.40 angstroms, respectively) while sinching in the binding pocket at segment 3 (average decrease of 0.95 angstroms). When BIM bound MCL-1 structures compared to the empty MCL-1 structures, the MCL-1 binding pocket displayed an even greater increase at segment 1 (average increase of 1.70 angstroms) and a slight increase at segment 2 (average increase of 0.10 angstroms) while sinching in the binding pocket at segment 3 (average decrease of 1.03 angstroms).

PyMOL is most confident with MCL-1^{L267V} structure prediction and least confident with MCL-1^{R214Q} structure prediction

The rotamer, or amino acid side chain orientation, with the greatest likelihood of occurrence is represented by the highest rotamer percentage on PyMOL. Additionally, the total number of rotamer states available in PyMOL. The total number of side chain orientations (rotamers) possible in PyMOL are listed in Table 1. The MCL-1^{R214Q} had the highest number of possible rotamers across all MCL-1 structures while the MCL-1^{L267V} had the lowest number of possible rotamers across all MCL-1 structures. The higher values may indicate that the true structure of the mutation is unpredictable as there are many orientations the side chain can adopt. On the other hand, the lower values associated with

the MCL-1^{L267V} mutation may indicate that the true structure of the mutation is more predictable as there are less orientations the side chain can adopt.

The most likely rotamer percentages were compiled across empty (2MHS), drug inhibitor bound (6OQC, 6OQB, 6FS0, 5LOF, and 6QYP), and BIM bound (2PQK, 6QFI, and 2KBW) MCL-1 structures for each of the mutation sites (Table 2). Across all the MCL-1 models bound to drug inhibitors and BIM, the R214Q mutation displayed the lowest rotamer percentages while the L267V displayed the greatest rotamer percentages. The low MCL-1^{R214Q} rotamer percentages are likely due to the change in charge required to mutate an arginine to a glutamine. Conversely, the relatively high L267V rotamer percentages are likely due to the conserved amino acid side chains between leucine and valine that allow for this mutagenesis to occur more readily.

The large structure of AZD5991 is in close proximity to MCL-1 amino acid changes

MCL-1^{WT} was overlaid and aligned with missense mutation MCL-1 models (Figures 11-16A). The impact of AZD5991's large, cyclic structure is especially clear in the alignment models of MCL-1^{WT} + MCL-1^{L186F} in which the drug inhibitor protrudes down in toward the L186F mutation site and affects the direction of the phenylalanine substitution (Figure 11). The close proximity of the AZD5991 drug is also apparent in the alignment models of MCL-1^{WT} & MCL-1^{L267V}. The Amgen176 drug displays a similar relationship with MCL-1^{L186F} & MCL-1^{L267V} mutation amino acid side chains and may display similar patterns of sensitivity to the AZD5991.

Similarly, the impact of BIM 2KBW's large size is clear in the alignment models of MCL-1^{WT} + MCL-1^{N223S} in which the BIM hangs down and into the N223S mutation site. This

affects the orientation of the Ser223 side chain as it points to the right side while the Ser223 in all other MCL-1^{N223S} models point to the left side (Figure 12).

The structure of MCL-1^{R214Q} & MCL-1^{V249L} are unpredictable

MCL-1^{WT} was overlaid and aligned of MCL-1^{R214Q} & MCL-1^{V249L} independently. In the MCL-1^{WT} + MCL-1^{R214Q} alignment models, the Q214 side chains were oriented in various directions without a clear pattern across the various MCL-1 structures (Figure 13). The unpredictable nature of the Gln214 side chain may be explained by the high total rotamer state / low rotamer percentages observed in Tables 1 & 2. The higher total rotamer states for MCL-1^{R214Q} hints at the unpredictable character of this mutation as there are many orientations the side chain can adopt (Table 1).

Valine and Leucine amino acid side chains share similar properties and structure; however, the MCL-1^{V249L} side chain orientations were not predictable. Especially in comparison to MCL-1^{L267V} mutation involving the same amino acids, MCL-1^{V249L} resulted in lower rotamer percentages than MCL-1^{L267V} (Table 2). These lower percentages indicate that the true structure of the mutation is unpredictable as there are more orientations the side chain can adopt. The MCL-1^{WT} + MCL-1^{V249L} alignment models reflect the rotamer data as the Leu249 side chain orientation is variable across the MCL-1 structures (Figure 14).

The L267V mutation prevents BIM displacement

The alignment feature on PyMOL was utilized to overlay WT MCL-1 structures over mutant MCL-1 models. More specifically, the closest distance of the most likely rotamers of the mutant amino acid side chains to drug inhibitors (Figure 15B - pink) and BIM activators

(Figure 15B - green) were measured using pairwise distances coded in Python (Supplementary Information). These distances were compared with the closest distances of the WT MCL-1 amino acid side chains to the drug inhibitors and BIM activators (Figure 15B). At the Leu267 residue, the distances from the drug inhibitors to the mutant valine amino acid side chain were less than the distances from the drug inhibitors to the WT leucine amino acid side chain. Conversely, the distances from the BIM activators to the mutant valine amino acid side chain were greater than the distances from the BIM to the WT leucine amino acid side chain. The shift in the mutant amino acid valine away from BIM may have effects on BIM displacement.

Murine MCL-1 has decreased binding affinity for MCL-1 compared to human MCL-1

The amino acid differences between murine and human MCL-1 were modeled on PyMOL by overlaying & aligning human MCL-1^{WT}, human MCL-1^{L267V}, and murine MCL-1. The two phenylalanines in murine MCL-1 at the human L246 and C286F sites are located on alpha helices 5 & 6 (Figure 16A). The cyclic side chain facing of the L246F murine model consistently faces in towards the binding pocket in all the MCL-1 structures. This bulky, cyclic amino acid side chain crowds the MCL-1 binding near the drug inhibitors (Figure 16B [5LOF, 6FS0, 6QYP, & 6OQC-A]). The bulky phenylalanine in murine MCL-1 could explain the decreased binding affinity of drug inhibitors compared to human MCL-1 in which the side chains do not exhibit as much steric hindrance.

The murine MCL-1's phenylalanine side chain is further away from the BIM compounds compared to the MCL-1 drug inhibitors (Figure 16B [6QFI, 2KBW, & 2PQK]). The increased distance between the BIM and murine MCL-1's phenylalanine side chain may

explain the strong binding affinity of BIM for murine MCL-1 observed in previous co-immunoprecipitation studies of MCL-1 and BIM (Figure 7).

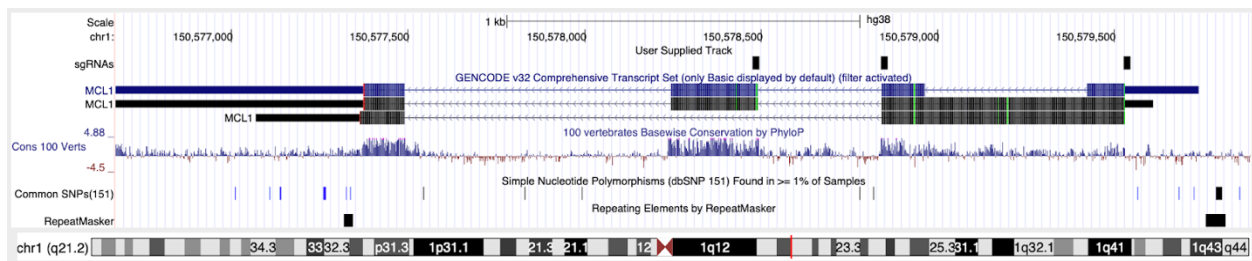


Figure 8. MCL-1 sgRNA guide sites. CRISPOR was utilized to design three forward (MCL1.tss1.f, MCL1.i2e2.f, and MCL1.e3i2.f) and reverse (MCL1.tss1.r, MCL1.i2e2r, and MCL1.e3i2.r) primer sets. Primer sets were designed to create guide RNA's targeting the intron/exon and 5' promoter/exon boundaries of MCL-1 to create a null endogenous MCL-1 protein while leaving the transfected, mutant MCL-1 cDNA unaffected.

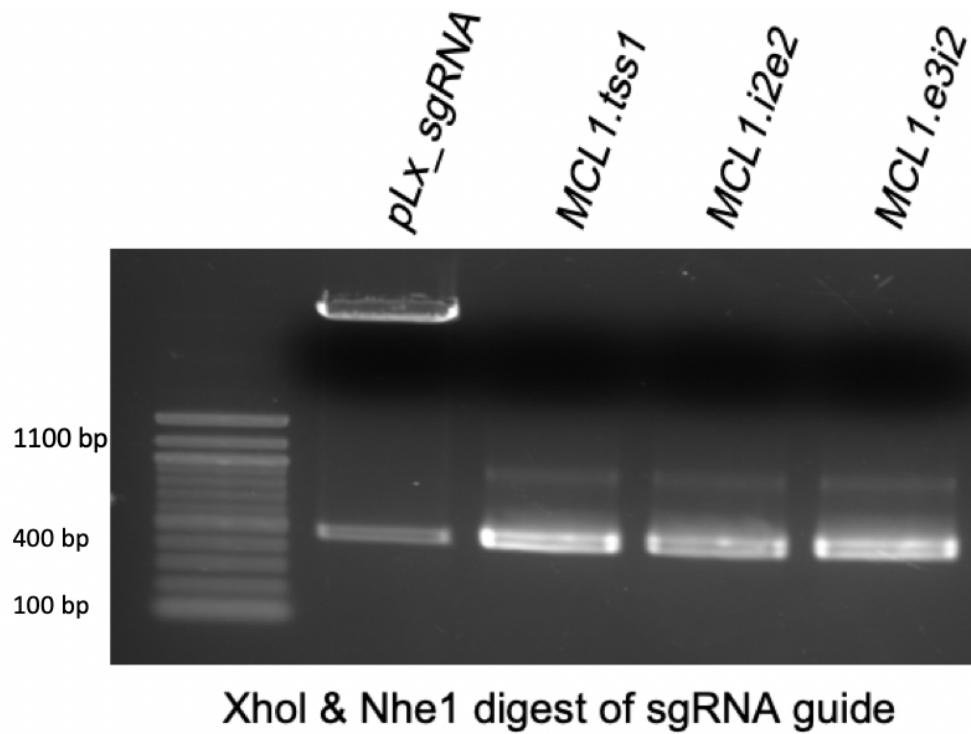


Figure 9. Xho1 & Nhe1 digest of sgRNA guides. Guide RNA's were analyzed for proper digestion and pure PCR product after the overlap extension PCR and Xho1 & Nhe1 digestion. The pLx_sgRNA plasmid and three sgRNA guides were visualized on ethidium bromide gel.

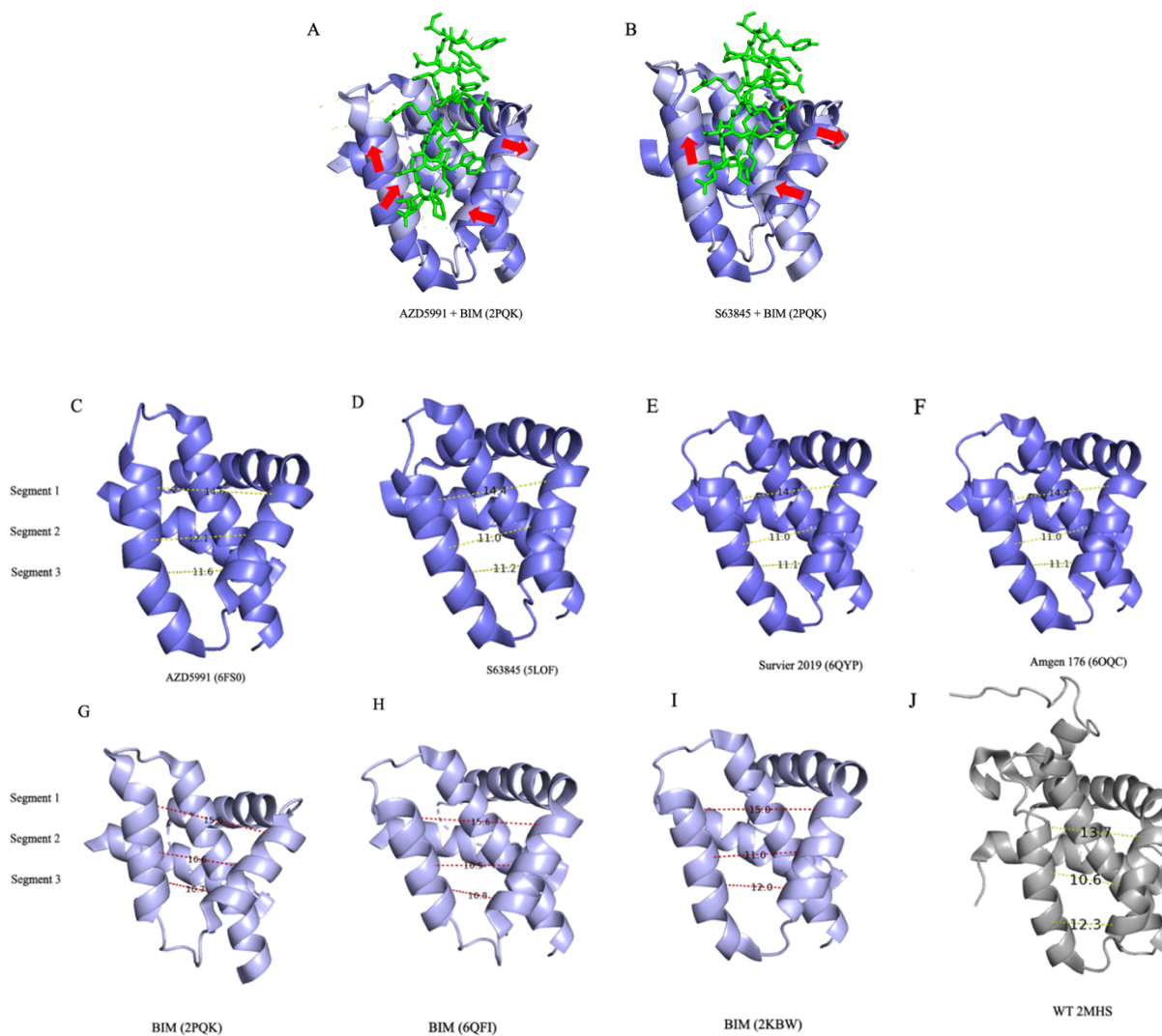


Figure 10. Drug inhibitors & BIM change MCL-1 structure. (A+B) Overlay & alignment models of drug inhibitors in complex with MCL-1 (dark purple) + BIM (green) in complex with MCL-1 (light purple) display a shift in MCL-1 structure. Specifically, the size of MCL-1 binding pocket in **(C-F)** drug inhibitor bound, **(G-I)** BIM bound, and **(J)** empty MCL-1 structures reveals that drug inhibitor binding widens the binding pocket at segment 1 (Ala227 to Val253). BIM binding widens the MCL-1 binding pocket at segment 1 even further while the segment 3 end of the binding pocket (Lys234 to Leu246) sinches during both drug inhibitor and BIM binding.

MCL1 Mutations	Empty MCL1	DRUG INHIBITORS						BIM Activators		
	2MHS	Amgen "176" inhibitor 9 (A): 6OQC	Amgen "176" inhibitor 9 (B): 6OQC	Amgen "176" inhibitor 10: 6OQB	AstraZeneca AZD5991 6FS0	Servier S63845 5LOF	Servier: 2019 6QYP	2PQK	6QFI	2KBW
L186F	20	5	5	5	5	5	5	5	5	10
R214Q	20	16	16	12	16	14	16	14	14	16
V216I	20	5	5	5	5	5	5	6	5	10
V216L	20	5	5	5	5	5	5	4	5	10
N223S	20	3	3	3	3	3	3	3	2	10
V249L	20	4	4	4	4	4	4	4	4	10
V258I	20	6	6	5	6	5	3	4	4	10
V258L	20	4	4	4	5	2	4	5	4	10
L267V	20	2	2	2	2	2	2	3	3	10
L267F	20	4	4	4	4	4	4	5	5	10

Table 1. PyMOL is most confident with MCL-1^{L267V} structure prediction and least confident with MCL-1^{R214Q} structure prediction. The total number of side chain orientations (rotamers) possible in PyMOL are listed. In general, the MCL-1^{R214Q} had the highest number of possible rotamers across all MCL-1 structures while the MCL-1^{L267V} had the lowest number of possible rotamers across all MCL-1 structures. The higher values indicate that the true structure of the mutation is unpredictable as there are many orientations the side chain can adopt and vis versa.

MCL1 Mutations	Empty MCL-1	DRUG INHIBITORS						BIM Activators		
	2MHS	Amgen "176" inhibitor 9 (A): 6OQC	Amgen "176" inhibitor 9 (B): 6OQC	Amgen "176" inhibitor 10: 6OQB	AstraZeneca AZD5991 6FS0	Servier S63845 5LOF	Servier 2019: 6QYP	2PQK	6QFI	2KBW
L186F	52.90%	61.70%	61.70%	61.70%	41.20%	52.90%	52.90%	61.70%	61.70%	61.70%
R214Q	23.00%	20.80%	20.80%	19.80%	20.80%	20.90%	17.80%	20.90%	20.90%	22.90%
V216I	52.70%	75.70%	67.50%	75.70%	69.00%	69.00%	69.00%	52.70%	69.00%	79.00%
V216L	80.00%	62.50%	73.80%	62.50%	66.30%	66.30%	66.30%	80.00%	66.30%	57.00%
N223S	57.30%	59.60%	59.30%	59.60%	78.70%	59.30%	59.60%	67.50%	76.80%	51.50%
V249L	57.00%	60.50%	60.50%	60.50%	60.50%	61.90%	47.40%	47.40%	47.40%	64.80%
V258I	79.10%	46.20%	53.40%	46.20%	65.80%	88.40%	72.40%	68.20%	69.70%	70.00%
V258L	92.30%	83.20%	68.20%	63.60%	74.30%	97.50%	50.00%	51.40%	51.80%	48.80%
L267V	98.60%	96.70%	96.70%	96.70%	98.30%	98.30%	98.30%	91.80%	92.50%	98.60%
L267F	86.20%	80.50%	80.50%	80.50%	76.00%	76.00%	76.00%	61.70%	52.90%	86.20%

Table 2. PyMOL is most confident with MCL-1^{L267V} structure prediction and least confident with MCL-1^{R214Q} structure prediction. Percentages corresponding to the most likely rotamers for various MCL-1 mutations. The generally low MCL-1^{R214Q} rotamer percentages may be due to a change in charge required to mutate an arginine to a glutamine. On the other hand, the relatively high L267V rotamer percentages are likely due to the conserved amino acid side chains between leucine and valine.

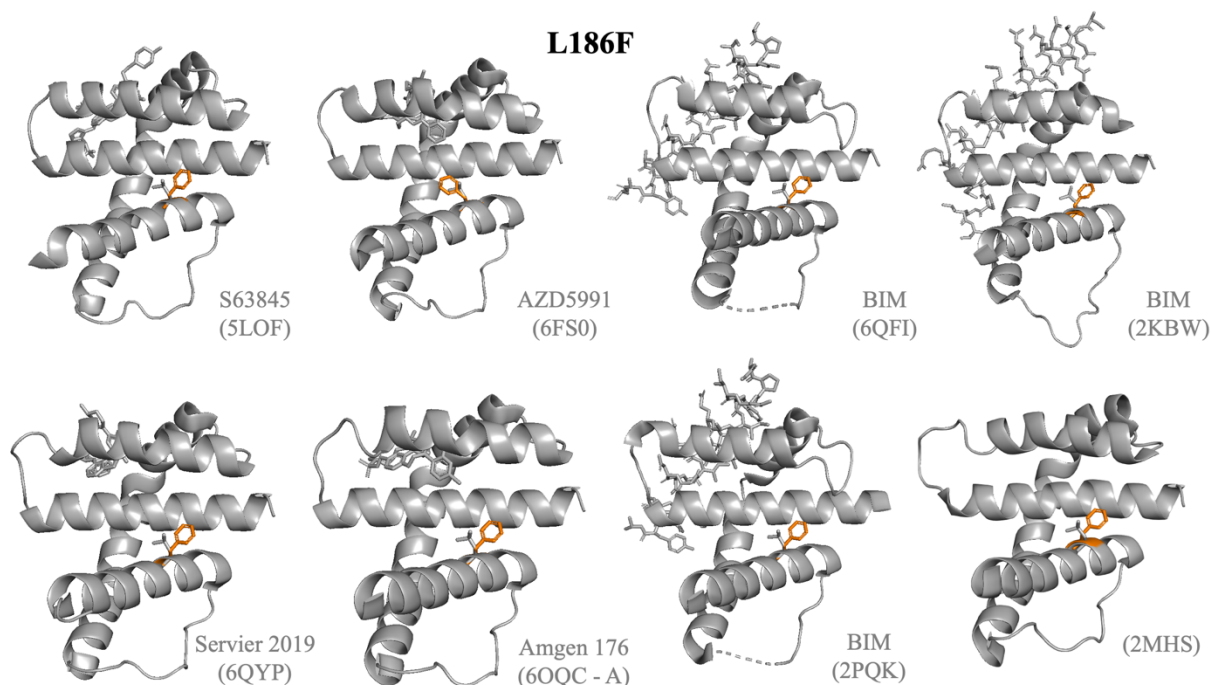


Figure 11. The large structure of AZD5991 is in close proximity to MCL-1 amino acid changes. Overlay & alignment models of MCL-1^{WT} (grey) + MCL-1^{L186F} (orange) in empty (2MHS), drug bound (5LOF, 6FS0, 6QYP, & 6OQC-A), and BIM bound (6QFI, 2KBW, & 2PQK) MCL-1 structures displays the protrusion of AZD5991 into the vicinity of the L186F amino acid mutation site. The large size of AZD5991 drug inhibitor causes MCL-1^{L186F} to lean in the opposite direction as the other MCL-1 structures.

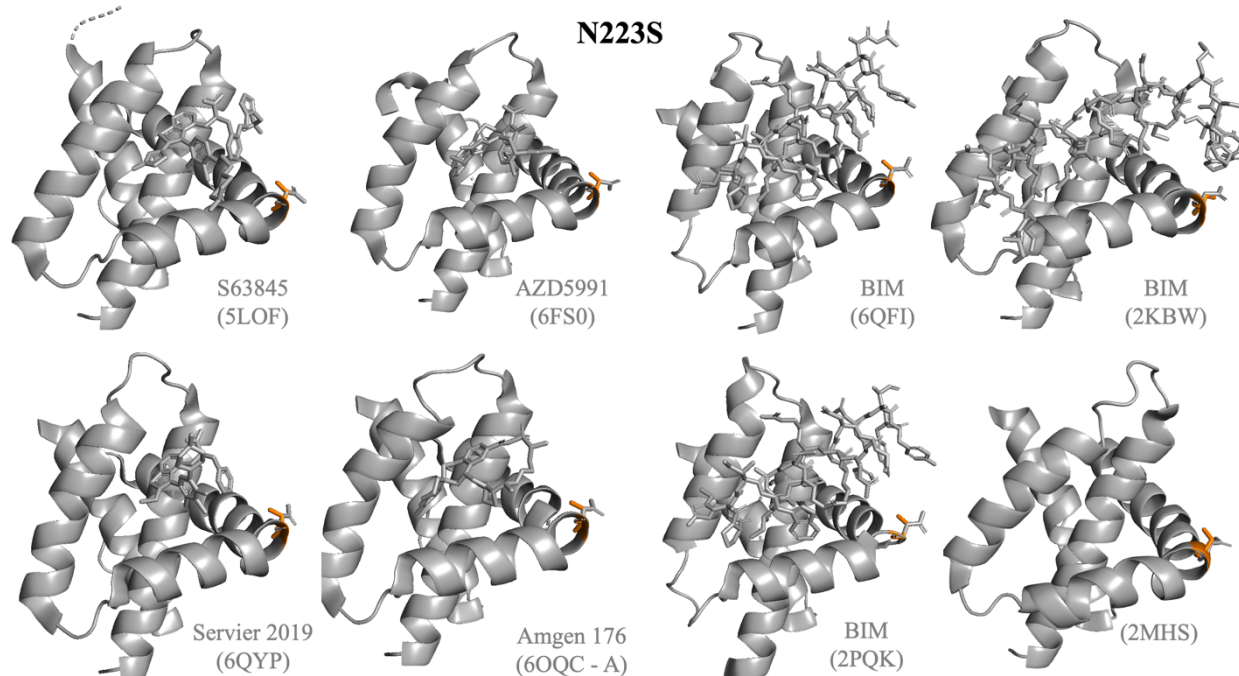


Figure 12. The large, overhanging structure of BIM 2KBW may affect the MCL-1 N223 residue. Overlay & alignment models of MCL-1^{WT} (grey) + MCL-1^{N223S} (orange) in empty (2MHS), drug bound (5LOF, 6FS0, 6QYP, & 6OQC-A), and BIM bound (6QFI, 2KBW, & 2PQK) MCL-1 structures reveals that BIM 2KBW is near the MCL-1 N223 residue. The large size of BIM 2KBW may be causing MCL-1^{N223S} to lean in the opposite direction as the other MCL-1 structures.

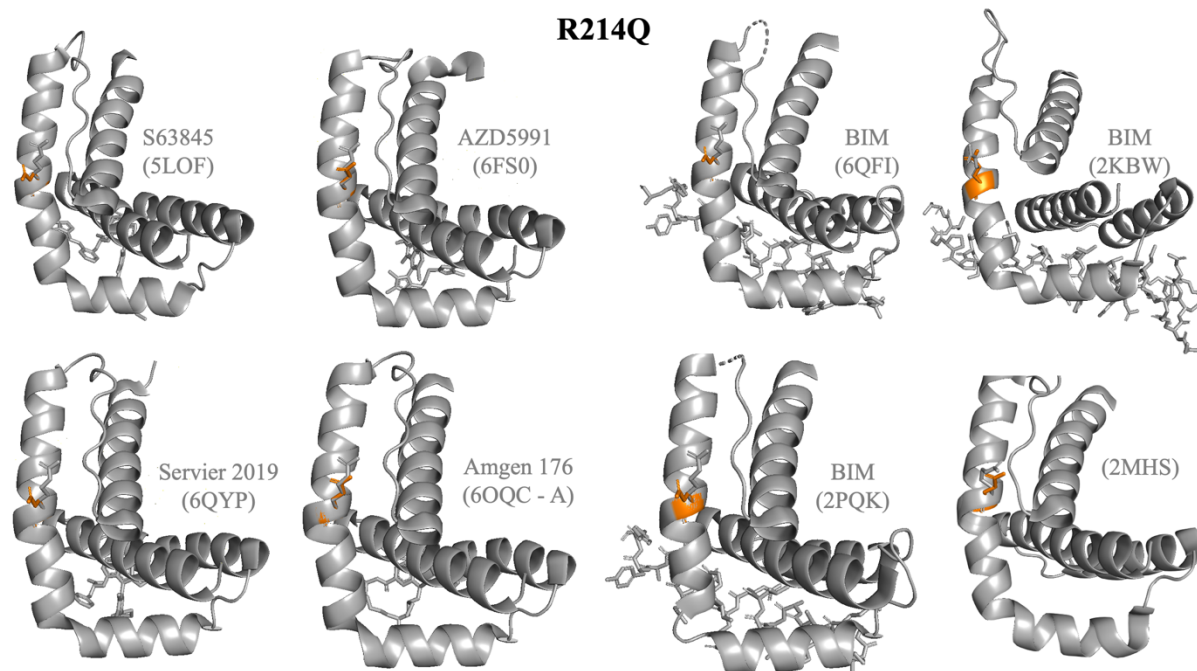


Figure 13. The structure of MCL-1^{R214Q} is unpredictable. Overlay & alignment models of MCL-1^{WT} (grey) + MCL-1^{R214Q} (orange) in empty (2MHS), drug bound (5LOF, 6FS0, 6QYP, & 6OQC-A), and BIM bound (6QFI, 2KBW, & 2PQK) MCL-1 structures do not display any clear side chain orientation patterns.

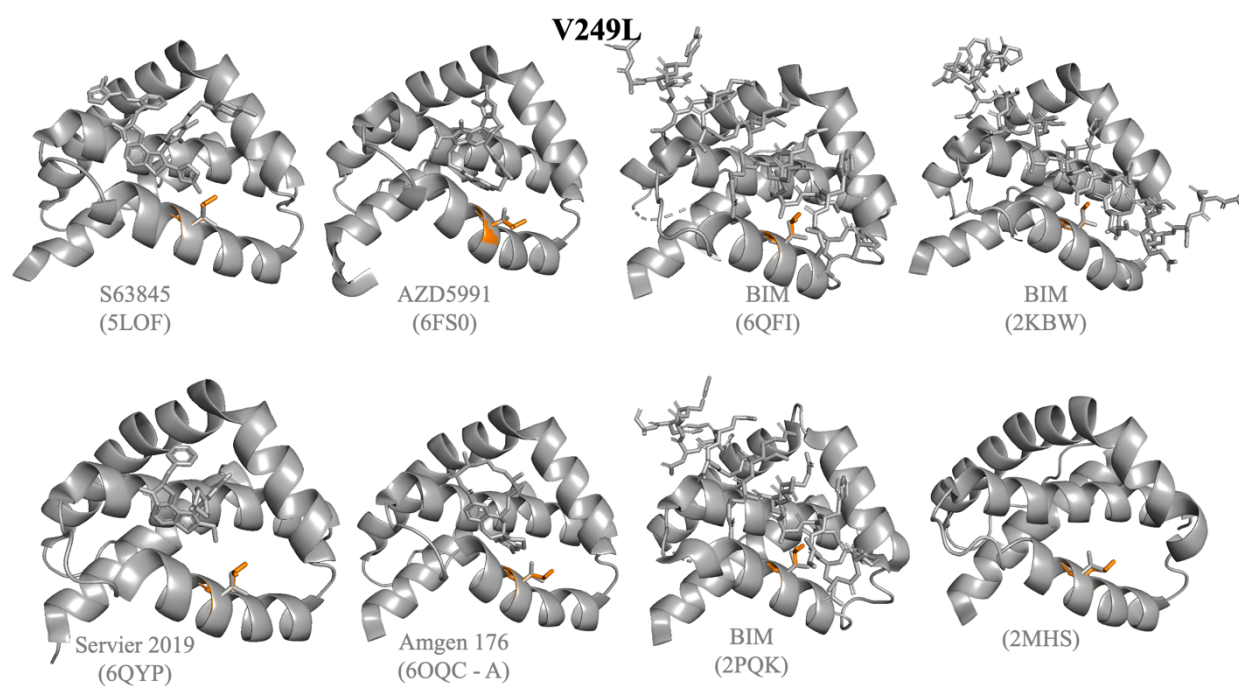


Figure 14. Despite the similarity in Valine & Leucine side chains, MCL-1^{V249L} structure is unpredictable. Overlay & alignment models of MCL-1^{WT} (grey) + MCL-1^{V249L} (orange) in empty (2MHS), drug bound (5LOF, 6FS0, 6QYP, & 6OQC-A), and BIM bound (6QFI, 2KBW, & 2PQK) MCL-1 structures do not display any clear patterns in side-chain orientation.

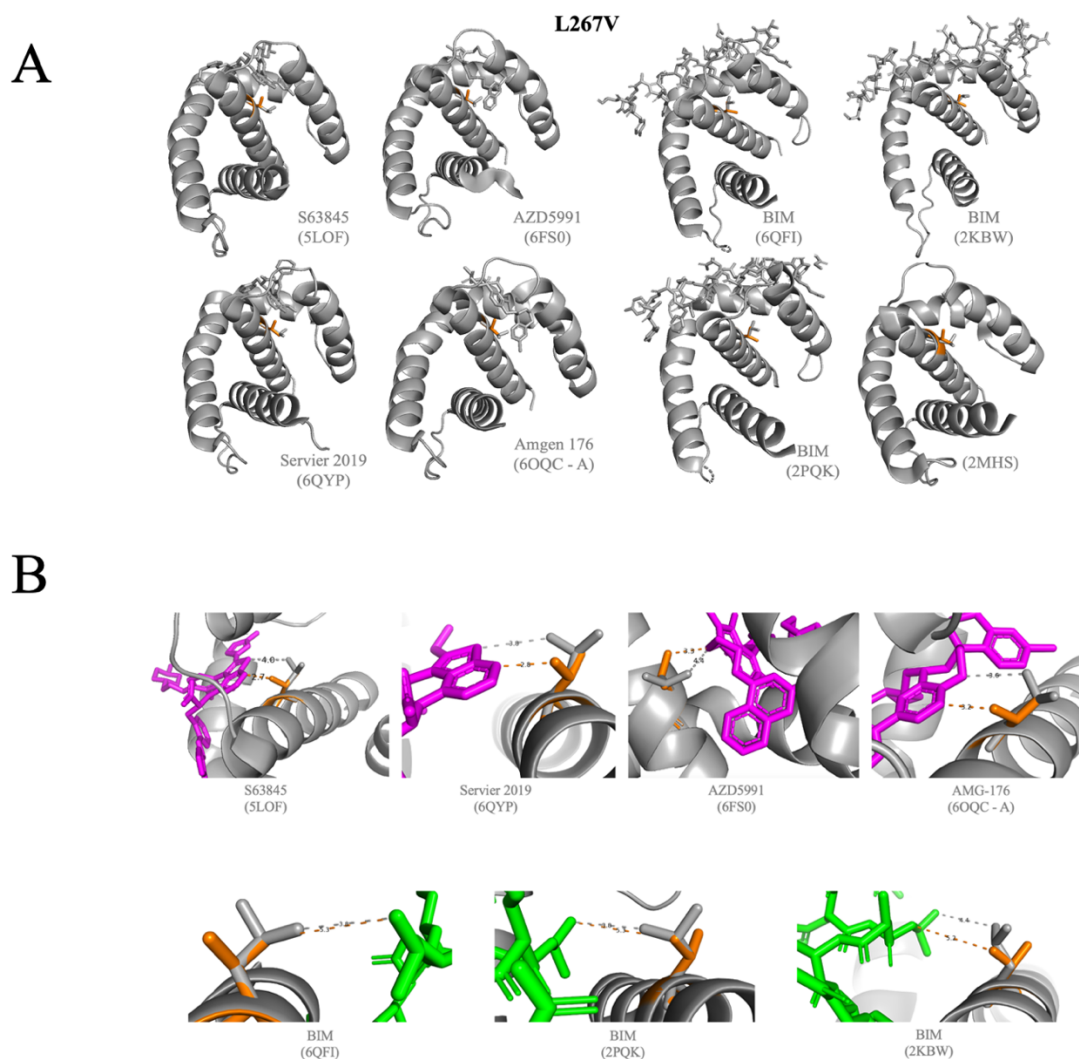


Figure 15. The MCL-1^{L267V} mutation prevents drug inhibitor binding & BIM displacement. (A) Overlay & alignment models of MCL-1^{WT} (grey) + MCL-1^{L267V} (orange) in empty (2MHS), drug bound (5LOF, 6FS0, 6QYP, & 6OQC-A), and BIM bound (6QFI, 2KBW, & 2PQK) MCL-1 structures display a difference in MCL-1^{WT} & MCL-1^{L267V} amino acid side chains between drug inhibitor and BIM bound structures. **(B)** Measurements of the shortest distance from the 267 residue to drug inhibitors and BIM reveal that MCL-1^{L267V} (orange) amino acid side chain shifts towards MCL-1 drug inhibitors (pink) and away from BIM (green).

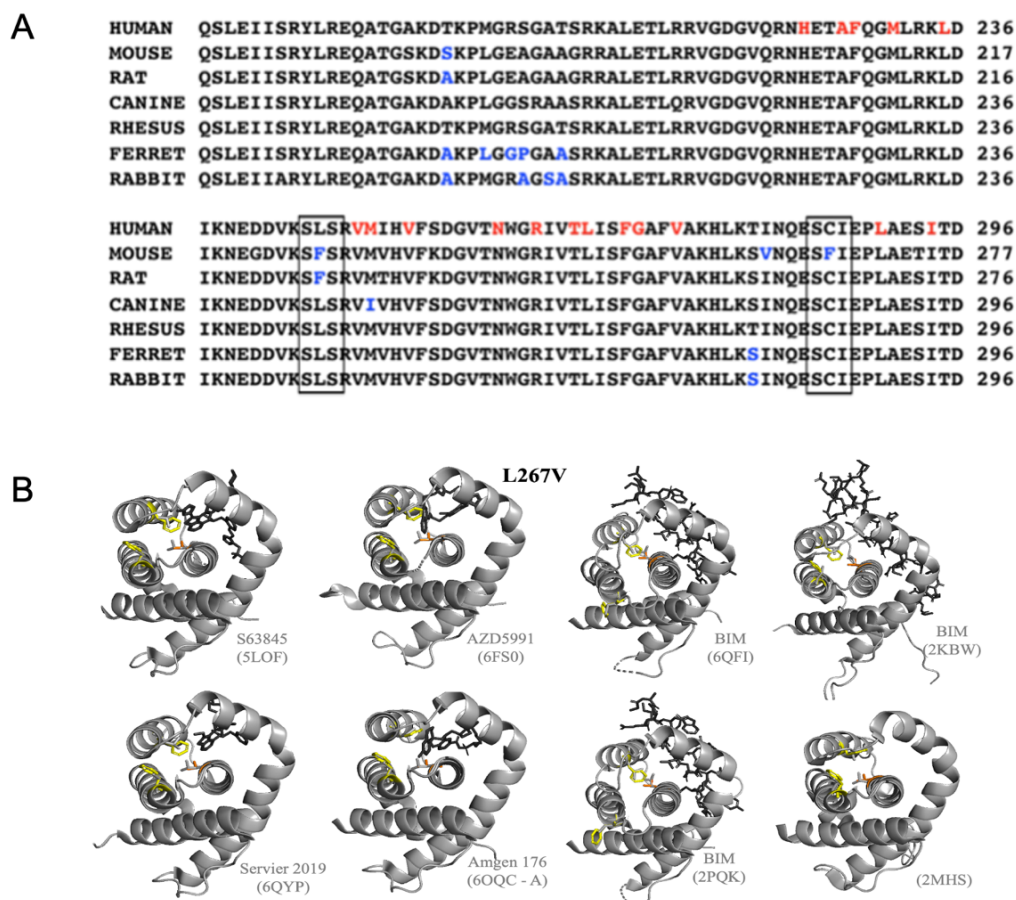


Figure 16. Murine MCL-1 has decreased binding affinity for MCL-1 inhibitors compared to human MCL-1 (A) Amino acid sequence alignment of MCL-1 across various vertebrate species. The amino acid differences in murine MCL-1 (human L246 to mouse F227 & human C267 to mouse F267) leads to an inability for all the current MCL1 inhibitors to bind efficiently to the BH3 binding pocket due to the large side aromatic group on phenylalanine. Figure derived from Zhao et al, *Biochemistry*, 2018³⁷. **(B)** Overlay & alignment of MCL-1^{WT} (grey) + MCL-1^{L267V} (orange) + murine MCL-1 (yellow) in empty (2MHS), drug bound (5LOF, 6FS0, 6QYP, & 6OQC-A), and BIM bound (6QFI, 2KBW, & 2PQK) MCL-1 structures displays murine phenylalanine near the drug inhibitors. Interaction between murine MCL-1 phenylalanine and drug inhibitors may prevent proper binding.

DISCUSSION:

Uncovering molecular mechanisms pertaining to the intrinsic apoptotic pathway in MM have opened doors for exploring specific proteins and regulators. MCL-1 is an essential anti-apoptotic protein for cell maintenance, survival, and regulated cell death within the BCL2 family. Furthermore, MCL-1 protein's BH regions form a binding pocket in which BH3 sensitizers and targeted therapy drugs can bind. The purpose of this experiment is to analyze the effects of MCL-1 amino acid substitutions on protein structure and function. It was predicted that MCL-1 amino acid substitutions may affect the protein's interactions with drugs inhibitors, BCL-2 family relative proteins, and even cell survival. With promising research uncovering the molecular mechanisms in MM, it is crucial that MCL-1 and targeted therapies are further investigated.

Modeling MCL-1 through PyMOL revealed conformational changes to the protein's structure. The binding of BIM to MCL-1 was found to change the shape of the binding pocket by altering the position of $\alpha 3$ & $\alpha 4$. More specifically, the measurements between $\alpha 3$ and $\alpha 4$ at three different segments exposed $\alpha 3$'s clockwise tilting when bound to BIM molecules (2PQK, 6QFI, and 2KBW). $\alpha 3$'s clockwise tilting caused a widening of the MCL-1 binding pocket around segment 1 and a narrowing of the binding pocket around segments 2 and 3. Fire et al.³⁸ have similarly observed a widening of the MCL-1 protein's binding groove. This conformational change of the MCL-1 protein may have significant implications for the efficacy of BH3 mimetics in their displacement of BIM and cell apoptosis³⁹.

PyMOL models of the MCL-1 mutations display changes in the amino acid side chains between the WT and mutant variants. In particular, the L267V amino acid substitution displayed changes in the side chain that may have implications for the binding of drug inhibitors and BIM. The Val267 associated with L267V was found to be closer in proximity to all drug inhibitors (6OQC, 6OQB, 6FS0, 5LOF, and 6QYP) (Figure 15B - pink); however, the Val267 side chain was also found to be further in distance to all the BIM molecules (2PQK, 6QFI, and 2KBW) (Figure 15B- green). The decrease in distance to the drug inhibitors is particularly interesting as the Valine side chains are smaller than the WT side chains in both amino acid substitutions. Furthermore, the properties of the amino acids are conserved after amino acids substitution as Leucine and Valine's side chains are both non-polar and aliphatic. Although the side chain substitutions are conserved in size and property, the L267V mutation is not exempt from phenotypic implications as these mutations alter the space available between the binding pocket and drug inhibitors & BIM molecules. These results are also supported by previous data that found that the MCL-1^{L267V} mutation does not induce the release of BIM bound to MCL-1 mutant (Figure 7). Denis et al.¹⁷ found that P2 and P3 were significant portions of MCL-1's hydrophobic groove in regard to ligand binding. In their study, Leu267 was identified as a hot spot or defining residue of the P2 pocket. Moreover, Leu267 was one of 11 MCL-1 binding site residues that contributed greater than 1 kcal/mol to binding free energy⁴⁰. Of the mutation sites investigated, the L267V amino acid substitution may affect the hydrophobic groove and the binding of BH3 mimetics and BIM.

The percentages associated with the most likely occurring rotamer revealed that MCL-1^{R214Q} amino acid substitution had the lowest likelihood of occurring at the true structural position while the L267V mutation had the highest likelihood of occurring at the true structural position. The high rotamer percentage in the L267V substitution may be explained by the conservation in size and property of the amino acid side chain. This may indicate that the L267V substitution is energetically favorable and structurally sound. Conversely, the low rotamer percentage in the R214Q substitution may be explained by the change of side chain property from a positively charged arginine to an uncharged glutamine. The relatively low rotamer percentages may indicate that the R214Q amino acid substitution is energetically unfavorable and structurally unsound. The electro-positivity and basicity formed by residues R214 and K215 in $\alpha 3$ & $\alpha 4$ distinguish MCL-1 from other anti-apoptotic proteins such as BCL-XL⁴¹. Day et al.⁴¹ also observed acidic residues from Puma and Noxa interacting with the basic K215 residue. In a similar manner, the R214 residue may have polar, acidic complements that have implications on ligand binding.

In addition to AZD5991's large, cyclic structure that occupies a larger surface area in the MCL-1 binding pocket and may affect sensitivity of the mutant MCL-1 proteins to AZD5991 drug, the steric hindrance of murine MCL-1's amino acid side chains was observed. The steric hindrance was caused by two phenylalanines at the human L246F and C286F sites that are located near the MCL-1 drug binding pocket (Figure 16). The bulky phenylalanines are near the drug inhibitors but are distant from the BIM activators. These figures confirmed previous findings and literature that support that murine MCL-1 has decreased binding affinity for MCL-1 compared to human MCL-1²².

CONCLUSION:

Although the structural effects of amino acid substitutions on the MCL-1 protein were observed through PyMOL analysis, the goal to study the effects of amino acid substitutions (V249L, L267V, N223S, and R214Q) on the MCL-1 protein's function was not yet tested. In order to study mutant MCL-1 protein function, the next step would be to insert mutant MCL-1 constructs into the MM cell lines and knock out endogenous MCL-1 through doxycycline inducible Cas 9. Additionally, molecular modeling of the PyMOL mutation structures would provide a more accurate model of the structures.

Taken together, the data suggests that MCL-1 mutations may affect the protein's interaction with drug inhibitors and alter the downstream intrinsic apoptotic pathway. As a protein that interacts directly with BH3 sensitizer drugs and cell survival, it is imperative that MCL-1 protein targeting therapy and the molecular mechanism of MM is further investigated.

Supplemental Information: Pairwise Distance Python Code

```

def pairwise_dist(sel1, sel2, max_dist, output="N", sidechain="N", show="N"):
    """
    usage: pairwise_dist sel1, sel2, max_dist, [output=S/P/N, [sidechain=N/Y,
    [show=Y/N]]]
    sel1 and sel2 can be any to pre-existing or newly defined selections
    max_dist: maximum distance in Angstrom between atoms in the two selections
    --optional settings:
    output: accepts Screen/Print/None (default N)
    sidechain: limits (Y) results to sidechain atoms (default N)
    show: shows (Y) individual distances in pymol menu (default=N)
    """
    print("")
    cmd.delete("dist*")
    extra=""
    if sidechain=="Y":
        extra=" and not name c+o+n"

    #builds models
    m1 = cmd.get_model(sel2+" around "+str(max_dist)+" and "+sel1+extra)
    m1o = cmd.get_object_list(sel1)
    m2 = cmd.get_model(sel1+" around "+str(max_dist)+" and "+sel2+extra)
    m2o = cmd.get_object_list(sel2)

    #defines selections
    cmd.select("__tsel1a", sel1+" around "+str(max_dist)+" and "+sel2+extra)
    cmd.select("__tsel1", "__tsel1a and "+sel2+extra)
    cmd.select("__tsel2a", sel2+" around "+str(max_dist)+" and "+sel1+extra)
    cmd.select("__tsel2", "__tsel2a and "+sel1+extra)
    cmd.select("IntAtoms_"+max_dist, "__tsel1 or __tsel2")
    cmd.select("IntRes_"+max_dist, "byres IntAtoms_"+max_dist)

    #controlers-1
    if len(m1o)==0:
        print("warning, '"+sel1+extra+"' does not contain any atoms.")
        return
    if len(m2o)==0:
        print("warning, '"+sel2+extra+"' does not contain any atoms.")
        return

    #measures distances
    s=""
    counter=0
    for c1 in range(len(m1.atom)):
        for c2 in range(len(m2.atom)):

```

```

        distance=math.sqrt(sum(map(lambda f: (f[0]-f[1])**2,
zip(m1.atom[c1].coord,m2.atom[c2].coord))))
        if distance<float(max_dist):
            s+="%s/%s/%s/%s/%s to %s/%s/%s/%s/%s: %.3f\n" %
(m1o[0],m1.atom[c1].chain,m1.atom[c1].resn,m1.atom[c1].resi,m1.atom[c1].name,m2o[0],m2
.atom[c2].chain,m2.atom[c2].resn,m2.atom[c2].resi,m2.atom[c2].name, distance)
            counter+=1
            if show=="Y": cmd.distance (m1o[0]+" and
"+m1.atom[c1].chain+"/"+m1.atom[c1].resi+"/"+m1.atom[c1].name, m2o[0]+" and
"+m2.atom[c2].chain+"/"+m2.atom[c2].resi+"/"+m2.atom[c2].name)

#controler-2
if counter==0:
    print("warning, no distances were measured! Check your selections/max_dist
value")
    return

#outputs
if output=="S":
    print(s)
if output=="P":
    f=open('IntAtoms_'+max_dist+'.txt','w')
    f.write("Number of distances calculated: %s\n" % (counter))
    f.write(s)
    f.close()
    print("Results saved in IntAtoms_%s.txt" % max_dist)
print("Number of distances calculated: %s" % (counter))
cmd.hide("lines", "IntRes_*")
if show=="Y": cmd.show("lines", "IntRes_"+max_dist)
cmd.deselect()

cmd.extend("pairwise_dist", pairwise_dist)

```

REFERENCES:

1. Seema, S. *et al.* Antitumor Activity of Thalidomide in Refractory Multiple Myeloma. *N. Engl. J. Med.* **7** (1999).
2. Boise, L. H., Kaufman, J. L., Bahlis, N. J., Lonial, S. & Lee, K. P. The Tao of myeloma. *Blood* **124**, 1873–1879 (2014).
3. Alexander, D. D. *et al.* Multiple myeloma: A review of the epidemiologic literature. *Int. J. Cancer* **120**, 40–61 (2007).
4. Hideshima, T. & Anderson, K. C. Molecular mechanisms of novel therapeutic approaches for multiple myeloma. *Nat. Rev. Cancer* **2**, 927–937 (2002).
5. Tai, Y.-T. *et al.* CRM1 inhibition induces tumor cell cytotoxicity and impairs osteoclastogenesis in multiple myeloma: molecular mechanisms and therapeutic implications. *Leukemia* **28**, 155–165 (2014).
6. Villalobos-Ortiz, M., Ryan, J., Mashaka, T. N., Opferman, J. T. & Letai, A. BH3 profiling discriminates on-target small molecule BH3 mimetics from putative mimetics. *Cell Death Differ.* **27**, 999–1007 (2020).
7. Cory, S. & Adams, J. M. The Bcl2 family: regulators of the cellular life-or-death switch. *Nat. Rev. Cancer* **2**, 647–656 (2002).
8. Kuwana, T. *et al.* BH3 Domains of BH3-Only Proteins Differentially Regulate Bax-Mediated Mitochondrial Membrane Permeabilization Both Directly and Indirectly. *Mol. Cell* **17**, 525–535 (2005).
9. Giam, M., Huang, D. C. S. & Bouillet, P. BH3-only proteins and their roles in programmed cell death. *Oncogene* **27**, S128–S136 (2008).
10. Montero, J. & Letai, A. Why do BCL-2 inhibitors work and where should we use them in the clinic? *Cell Death Differ.* **25**, 56–64 (2018).
11. Czabotar, P. E. *et al.* Bax Crystal Structures Reveal How BH3 Domains Activate Bax and Nucleate Its Oligomerization to Induce Apoptosis. *Cell* **152**, 519–531 (2013).
12. Slomp, A. *et al.* Multiple myeloma with 1q21 amplification is highly sensitive to MCL-1 targeting. *Blood Adv.* **3**, 4202–4214 (2019).
13. Yadav, N. *et al.* Molecular insights on cytochrome c and nucleotide regulation of apoptosome function and its implication in cancer. *Biochim. Biophys. Acta Mol. Cell Res.* **1867**, 118573 (2020).
14. Smith, V. M. *et al.* Specific interactions of BCL-2 family proteins mediate sensitivity to BH3-mimetics in diffuse large B-cell lymphoma. *Haematologica* **105**, 2150–2163 (2020).
15. Aouacheria, A., Rech de Laval, V., Combet, C. & Hardwick, J. M. Evolution of Bcl-2 homology motifs: homology versus homoplasy. *Trends Cell Biol.* **23**, 103–111 (2013).
16. Sattler, M. *et al.* Structure of Bcl-xL-Bak peptide complex: recognition between regulators of apoptosis. *Science* **275**, 983–986 (1997).
17. Denis, C., Sopková-de Oliveira Santos, J., Bureau, R. & Voisin-Chiret, A. S. Hot-Spots of Mcl-1 Protein. *J. Med. Chem.* **63**, 928–943 (2020).
18. Petros, A. M. *et al.* Rationale for Bcl-xL/Bad peptide complex formation from structure, mutagenesis, and biophysical studies. *Protein Sci. Publ. Protein Soc.* **9**, 2528–2534 (2000).
19. Juin, P., Geneste, O., Gautier, F., Depil, S. & Campone, M. Decoding and unlocking the BCL-2 dependency of cancer cells. *Nat. Rev. Cancer* **13**, 455–465 (2013).
20. Glantz-Gashai, Y., Meirson, T., Reuveni, E. & Samson, A. O. Virtual screening for potential inhibitors of Mcl-1 conformations sampled by normal modes, molecular dynamics, and nuclear magnetic resonance. *Drug Des. Devel. Ther.* **11**, 1803–1813 (2017).

21. Belmar, J. & Fesik, S. W. Small molecule Mcl-1 inhibitors for the treatment of cancer. *Pharmacol. Ther.* **145**, 76–84 (2015).
22. Bolomsky, A. *et al.* MCL-1 inhibitors, fast-lane development of a new class of anti-cancer agents. *J. Hematol. Oncol. J Hematol Oncol* **13**, 173 (2020).
23. Gouill, S. L., Podar, K., Harousseau, J.-L. & Anderson, K. C. Mcl-1 Regulation and Its Role in Multiple Myeloma. *Cell Cycle* **3**, 1259–1262 (2004).
24. Gandhi, V., Balakrishnan, K. & Chen, L. S. Mcl-1: the 1 in CLL. *Blood* **112**, 3538–3540 (2008).
25. Wu, X., Luo, Q. & Liu, Z. Ubiquitination and deubiquitination of MCL1 in cancer: deciphering chemoresistance mechanisms and providing potential therapeutic options. *Cell Death Dis.* **11**, 1–11 (2020).
26. Warren, C. F. A., Wong-Brown, M. W. & Bowden, N. A. BCL-2 family isoforms in apoptosis and cancer. *Cell Death Dis.* **10**, 1–12 (2019).
27. Opferman, J. T. *et al.* Development and maintenance of B and T lymphocytes requires antiapoptotic MCL-1. *Nature* **426**, 671–676 (2003).
28. Wuillème-Toumi, S. *et al.* Mcl-1 is overexpressed in multiple myeloma and associated with relapse and shorter survival. *Leukemia* **19**, 1248–1252 (2005).
29. Gu, W.-W., Wang, J.-S., Mu, K. & Ren, G. [Influence of Combination with 1q21 Amplification or-No in Patients with Newly Diagnosed MM on the Clinical Efficacy of Bortezomib-based induction chemotherapy and Long-Term Prognosis of Patients]. *Zhongguo Shi Yan Xue Ye Xue Za Zhi* **28**, 1251–1255 (2020).
30. Gélinas, C. & White, E. BH3-only proteins in control: specificity regulates MCL-1 and BAK-mediated apoptosis. *Genes Dev.* **19**, 1263–1268 (2005).
31. Yang, C.-Y. & Wang, S. Analysis of Flexibility and Hotspots in Bcl-xL and Mcl-1 Proteins for the Design of Selective Small-Molecule Inhibitors. *ACS Med. Chem. Lett.* **3**, 308–312 (2012).
32. Niu, X. *et al.* Binding of released Bim to Mcl-1 is a mechanism of intrinsic resistance to ABT-199 which can be overcome by combination with daunorubicin or cytarabine in AML cells. *Clin. Cancer Res. Off. J. Am. Assoc. Cancer Res.* **22**, 4440–4451 (2016).
33. Merino, D. *et al.* BH3-Mimetic Drugs: Blazing the Trail for New Cancer Medicines. *Cancer Cell* **34**, 879–891 (2018).
34. Albershardt, T. C. *et al.* Multiple BH3 Mimetics Antagonize Antiapoptotic MCL1 Protein by Inducing the Endoplasmic Reticulum Stress Response and Up-regulating BH3-only Protein NOXA. *J. Biol. Chem.* **286**, 24882–24895 (2011).
35. Roberts, A. W. & Huang, D. Targeting BCL2 With BH3 Mimetics: Basic Science and Clinical Application of Venetoclax in Chronic Lymphocytic Leukemia and Related B Cell Malignancies. *Clin. Pharmacol. Ther.* **101**, 89–98 (2017).
36. Lin, V. S., Xu, Z.-F., Huang, D. C. S. & Thijssen, R. BH3 Mimetics for the Treatment of B-Cell Malignancies—Insights and Lessons from the Clinic. *Cancers* **12**, (2020).
37. Zhao, B. *et al.* Understanding the Species Selectivity of Myeloid Cell Leukemia-1 (Mcl-1) Inhibitors. *Biochemistry* **57**, 4952–4958 (2018).
38. Fire, E., Gullá, S. V., Grant, R. A. & Keating, A. E. Mcl-1–Bim complexes accommodate surprising point mutations via minor structural changes. *Protein Sci. Publ. Protein Soc.* **19**, 507–519 (2010).
39. Liu, Q. *et al.* Bim escapes displacement by BH3-mimetic anti-cancer drugs by double-bolt locking both Bcl-XL and Bcl-2. *eLife* **8**,

40. Marimuthu, P. & Singaravelu, K. Prediction of Hot Spots at Myeloid Cell Leukemia-1–Inhibitor Interface Using Energy Estimation and Alanine Scanning Mutagenesis. *Biochemistry* **57**, 1249–1261 (2018).
41. Day, C. L. *et al.* Structure of the BH3 domains from the p53-inducible BH3-only proteins Noxa and Puma in complex with Mcl-1. *J. Mol. Biol.* **380**, 958–971 (2008).